eNeuro

Research Article: New Research* | *Disorders of the Nervous System

Alpha-synuclein aggregates increase the conductance of substantia nigra dopamine neurons, an effect partly reversed by the KATP channel inhibitor glibenclamide

https://doi.org/10.1523/ENEURO.0330-20.2020

Cite as: eNeuro 2020; 10.1523/ENEURO.0330-20.2020

Received: 27 July 2020
Revised: 13 October 2020
Accepted: 18 October 2020

Alpha-synuclein aggregates increase the conductance of substantia nigra dopamine neurons, an effect partly reversed by the KATP channel inhibitor glibenclamide.

E. Hill[1], R. Gowers[2,3], M. J. E. Richardson[2], M. J. Wall[1*]

[1] School of Life Sciences, Gibbet Hill Campus, University of Warwick, CV4 7AL

[2] Warwick Mathematics Institute, University of Warwick, CV4 7AL

[3] Institute for Theoretical Biology, Department of Biology, Humboldt-Universität zu Berlin, Philippstraße 13, Haus 4, 10115, Berlin, Germany

[*] Corresponding author:

Dr Mark Wall

School of Life Sciences

University of Warwick

CV4 7AL

Mark.wall@warwick.ac.uk

Author contributions: EH and MJW designed the experiments. EH performed the experiments. EH, RG and MJER analysed the data. EH, MJER and MJW wrote the manuscript.

Funding: EH holds a BBSRC-funded PhD Studentship. RG held an EPSRC funded PhD studentship.

Conflicts of Interest: The authors declare that there are no competing or conflicting interests

Abstract

Dopaminergic neurons in the substantia nigra pars compacta (SNpc) form an important part of the basal ganglia circuitry, playing key roles in movement initiation and co-ordination. A hallmark of Parkinson's disease (PD) is the degeneration of these SNpc dopaminergic neurons leading to akinesia, bradykinesia and tremor. There is gathering evidence that oligomeric alpha synuclein (α-syn) is one of the major pathological species in PD, with its deposition in Lewy bodies closely correlated with disease progression. However the precise mechanisms underlying the effects of oligomeric α-syn on dopaminergic neuron function have yet to be fully defined. Here we have combined electrophysiological recording and detailed analysis to characterise the time-dependent effects of α-syn aggregates (consisting of oligomers and possibly small fibrils) on the properties of SNpc dopaminergic neurons. The introduction of α-syn aggregates into single dopaminergic neurons via the patch electrode significantly reduced both the input resistance and the firing rate without changing the membrane potential. These effects occurred after 8-16 minutes of dialysis but did not occur with the monomeric form of α-syn. The effects of α-syn aggregates could be significantly reduced by pre-incubation with the ATP-sensitive potassium channel (KATP) inhibitor glibenclamide. This data suggests that accumulation of α-syn aggregates in dopaminergic neurons may chronically activate KATP channels leading to a significant loss of excitability and dopamine release.

Significance statement

Alpha synuclein oligomers are one of the key toxic species in Parkinson's disease, with their accumulation leading to dopamine neuron dysfunction. Introducing alpha synuclein

aggregates (oligomers and possibly small fibrils) into single substantia nigra dopamine neurons led to a marked increase in whole cell conductance and a corresponding fall in the firing rate. These changes were diminished by inhibiting ATP-sensitive K channels. Thus, the build-up of alpha synuclein oligomers during the progression of Parkinson's disease could chronically shunt dopamine neurons, via channel activation (which may include KATP channel activation) to reduce dopamine release.

Introduction

Mid-brain dopaminergic neurons (DNs) play major roles in the control of movement, emotion, arousal and reward behaviour. They possess large numbers of projections, have pacemaker activity (firing action potentials at rest) and are therefore highly energy intensive. This makes them particularly sensitive to oxidative damage (which can lead to mitochondrial dysfunction, Michel et al, 2016) and they are the most susceptible to degeneration in Parkinson's disease (PD, Damier et al, 1999). DNs are lost over the progression of PD, primarily from the substantia nigra pars compacta (SNpc) but later in the disease there is also loss from the ventral tegmental area (VTA). Symptoms of PD only become apparent when 70-80 % of the dopamine input to the striatum is lost (Bernheimer et al, 1973) making it difficult to detect PD at early stages. Understanding what happens to these dopaminergic neurons early in pathology is important as it could provide improved diagnosis and potentially new targets to prevent or slow disease progression.

Alpha synuclein (α-syn) is a small, native intracellular protein, found primarily at presynaptic terminals (Iwai et al, 1995) where it contributes to neurotransmitter uptake and vesicle recycling. It can also localise to the mitochondria and the nucleus (Burre et al, 2010). Molecules of α-syn are intrinsically disordered (Alderson and Markley, 2013) but can become ordered upon aggregation, triggering a pathological cascade. First α-syn aggregates into soluble oligomers (dimers and trimers) and then it can go on to form longer fibrils and ultimately it can form insoluble Lewy Bodies (LB; Spillantini et al, 1997). Lewy bodies are a key pathological marker in the brains of PD patients with their abundance correlating with disease severity. LB formation involves a complex interplay between α-syn fibrillization, post-translational modifications, and interactions of α-syn aggregates with membranous organelles. LB formation can lead to the disruption of mitochondrial function, to synapse dysfunction and of a decline in general cell function (Mahul-Mellier et al. 2020). However, there is also evidence that the small soluble oligomers contribute to toxicity (Winner et al, 2011; reviewed in Bengoa-Vergniory et al, 2017). At the presynaptic terminal, oligomeric α-syn can induce synaptic dysfunction by disrupting vesicle trafficking (Jakes et al, 1994). It also interferes with synaptobrevin in the SNARE complex which is vital for the fusion of vesicles with the plasma membrane for neurotransmitter release (Burre et al, 2010; Murphy et al, 2000; Lashuel et al, 2013). Kaufmann et al (2016) showed that α-syn oligomers reduced the excitability and input resistance of cortical pyramidal cells.

In this study, we have used whole-cell patch-clamp recording to provide a detailed characterisation of the electrophysiological effects of introducing aggregated α-syn (oligomers plus a small proportion of fibrils) into single dopaminergic neurons in the substantia nigra of mouse brain slices. Since the α-syn aggregates are only introduced into one neuron, there will be no compensation within the circuit and any slow cellular uptake steps (which may occur if α-syn aggregates were applied extracellularly) are removed. Each cell acts as its own internal control, as at the time of whole-cell breakthrough the α-syn aggregates will not have diffused into the neuron This approach has successfully been used to examine the effects of oligomeric tau on pyramidal neurons (Hill et al, 2019) and the effects of α-syn oligomers on layer-V pyramidal cells in the neocortex (Kaufmann et al, 2016).

As well as using standard-IV relationships (with step-current injections) to measure the changes in dopaminergic neuron electrophysiology, we have also utilised the dynamic-IV protocol. This was originally applied with cortical pyramidal neurons and interneurons (Badel et al, 2008a; Badel et al, 2008b; Harrison et al, 2015) and can be used to develop simplified, but empirically verified quantitative models of their responses. Though the cortical cells in the original study exhibit non-linear voltage and calcium-activated currents, under ongoing *in-vivo*-like fluctuating current stimulation their response could be well captured by an effective linear I-V curve (away from action potential threshold). Dopaminergic neurons, however, have more strongly expressed non-linearities (Richards et al, 1997; Neuhoff et al 2002), and it can therefore be anticipated that the resulting dynamic-IV curves will diverge from an Ohmic linear form below threshold. Despite this, we have determined that the dynamic IV can still be used to accurately extract a number of key electrophysiological parameters.

Using these approaches, we have characterised the real-time effects of α-syn aggregates on the electrophysiological properties of single neurons. We find that their major effect is to induce an increase in whole-cell conductance, which significantly dampens neuronal excitability and firing rate. These effects were partially but significantly reduced by glibenclamide, an ATP-sensitive K channel inhibitor, suggesting a role for these channels in the pathological actions of α-syn aggregates.

Methods

Preparation of acute brain slices

All experiments were approved by the local Animals Welfare and Ethics Board (AWERB) at the University of Warwick. C57/Bl6 mice (2-3 weeks; of either sex) were killed by cervical dislocation and decapitated in accordance with the U.K. Animals (Scientific Procedures) Act (1986). The brain was rapidly dissected and kept on ice. The cerebellum was removed, and the rostral section of the brain was trimmed. The brain was then mounted rostral side down. Coronal slices (350 μM) were cut with a Microm HM 650V microslicer in cold (2-4°C) high Mg^{2+}, low Ca^{2+} aCSF, composed of (mM): 127 NaCl, 1.9 KCl, 8 $MgCl_2$, 0.5 $CaCl_2$, 1.2 KH_2PO_4, 26 $NaHCO_3$, 10 D-glucose (pH 7.4 when bubbled with 95% O_2 and 5% CO_2, 300 mOSM). Slices were stored at 34 °C in standard aCSF (1 mM Mg^{2+} and 2 mM Ca^{2+}) for at least 1 hour before recording and were viable for up to 8 hours.

Preparation of alpha synuclein aggregates

Recombinant human alpha-synuclein protein aggregates were purchased from Abcam (ab218819). These aggregates are advertised as pre-formed fibrils (PFFs) which was confirmed using negative-stain electron microscopy. Since we wanted to introduce smaller oligomeric species of alpha synuclein into neurons, the PFFs were first broken down into smaller aggregates before recordings were made. PFF samples were sonicated (as in Polinski et al, 2018) for 15 minutes (50-60 Hz) at room temperature using a Grant Ultrasonic XUBA1 bath. . Recombinant human alpha-synuclein protein in monomeric form (ab218818) was used as a control and negative-stain electron microscopy was used to confirm it was not aggregated.

Transmission electron microscopy

Formvar/carbon-coated 300-mesh copper grids (#S162, Agar Scientific) were glow-discharged using the ELMO system from Cordouan Technologies. Five microliters of alpha synuclein species (monomer, PFF or sonicated PFFs) were pipetted onto the grid and allowed to bind for 1 min. Excess samples were removed with a strip of filter paper, and 5 µl of 2% uranyl acetate added for 1 min. After removing the excess stain with a strip of filter paper, the grids were imaged using a JEOL-2100F transmission electron microscope.

Whole-cell patch-clamp recording

A slice was transferred to the recording chamber, submerged and perfused (2-3 ml/min^{-1}) with aCSF at 30-32 °C. Slices were visualized using IR-DIC optics with an Olympus BX151W microscope (Scientifica, Bedford UK) and a CCD camera (Hitachi). Whole-cell current-clamp recordings were made from dopaminergic neurons in the substantia nigra pars compacta using patch pipettes (5–10 MΩ) manufactured from thick-walled glass (Harvard Apparatus, Edenbridge, UK). Intracellular solution was filtered before use (0.2 µm) and contained in (mM): potassium gluconate 135, NaCl 7, HEPES 10, EGTA 0.5, phosphocreatine 10, MgATP 2, NaGTP 0.3, 293 mOSM, pH 7.2). The intracellular solution was filtered (2-4 μm) before the addition of α-syn aggregates (2 µl of a 69 µM stock into 275 µl intracellular solution to give final concentration of 500 nM) as filtering reduces the aggregate concentration (Hill et al, 2020; Kaufmann et al, 2016). The molar concentrations of alpha-synuclein species are based on the molar mass of monomeric alpha-synuclein (14 kD) due to the likelihood that samples will contain a range of aggregate sizes. This method has been used in similar studies (see Hill et al, 2019 and Thakur et al, 2019) and will result in an overestimate of aggregate concentration. For example if aggregates are on average tetramers, then the concentration of aggregates will be 4x lower than reported. A subset of neurons were filled with AF594 dye (50 μM) via the patch pipette for immunohistochemistry. Voltage recordings were made using an Axon Multiclamp 700B amplifier (Molecular Devices, USA) and digitised at 20 KHz. Data acquisition and analysis were performed using pClamp 10 (Molecular Devices). Recordings from neurons that had a resting membrane potential of between -55 and – 75 mV at whole-cell breakthrough were accepted for analysis. The bridge balance was monitored throughout the experiments and any recordings where it changed by more than 20 % were discarded.

Stimulation Protocols

Standard IV protocol: Standard current-voltage relationships (SIV) were constructed by injecting step currents (3 s duration, with a 5 s interval) starting at -200 pA and then incrementing by either 50 or 100 pA until a regular firing pattern was induced.

Naturalistic current injection: A naturalistic, fluctuating current (40 s duration, see below for details) was injected into neurons and the resulting voltage trace was used to measure the frequency of action-potential firing (using threshold detection in Clampfit).

Immunohistochemistry

After completing the electrophysiology recordings from dopaminergic neurons, with the addition of AF594 dye (50 μM) in the patch pipette, slices (350 μM) were fixed in 4% PFA for 45 minutes at room temperature and then overnight at 4ºC. The tissue was then washed 5 times for 5 minutes with PBS. The slices were then blocked for an hour (1% BSA, 0.4% Triton 100X in PBS, 400 μl per slice) then washed 3 times for 5 minutes with PBS. The primary antibodies against tyrosine hydroxylase (1:1000, Sheep), was added to the slices (250 μl per slice) for an hour at room temperature and then kept at 4-8ºC overnight. Slices were washed 5 times for 5 minutes with PBS and then the secondary antibody was added (anti-sheep 488, 1:500, 200 μl per slice) for 4 hours at room temperature. The slices were then washed 5 times for 5 minutes with PBS, and then mounted on glass slides with Vectashield (Vector laboratories, Peterborough UK). All imaging was carried using confocal microscopy (Leica 710 and Zen Black for image acquisition and processing). Controls were carried out without incubating with the primary antibodies and showed no fluorescence.

Drugs and substances

Recombinant human alpha-synuclein aggregates were purchased from Abcam (ab218819) along with the corresponding monomers (ab218818). Dopamine (HB1835) and ZD 7288 (HB1152) were purchased from Hello Bio (HB1835). Glibenclamide (PHR1287) was purchased from Sigma-Aldrich. The Sheep polyclonal Anti-Tyrosine hydroxylase was purchased from Merck (AB1542) and Donkey anti-sheep 488 secondary from Invitrogen (A11015). The Alexa Fluor 594 hydrazide dye was purchased from Molecular Probes (10072752).

Statistics

Each recorded cell is one data point. All experimental conditions were measured using multiple animals as only 1 cell was recorded per slice and recording conditions were interleaved to remove bias introduced from individual animals. Data points for each experimental condition were derived from a minimum of 4 individual animals (the exact numbers are provided in the figure legends). Statistical analysis was performed using non parametric methods: Kruskal–Wallis one-way analysis of variance (ANOVAs), Mann Whitney and Wilcoxon signed-rank tests as required. All data is represented as mean and standard error of the mean with individual experiments represented by single data points. Standard deviations are given in table 1.

Neuronal parameter extraction

Both the standard IV-curve (response to constant current inputs) and dynamic IV-curve (Badel et al, 2008) methods were used to extract estimates for the cellular conductance under the various pharmacological conditions. The voltage was modelled by the following the current-balance equation

$$C\frac{dV}{dt} + I_{ion} = I_{inj} \qquad \text{Eq 1}$$

where C is the capacitance, I_{ion} is the summed intrinsic current (including voltage-gated and calcium-gated currents) and I_{inj} in the current injected via the electrode during the different protocols. All computational modelling and data-fitting was carried out using custom written code in the Julia language (Bezanson et al, 2014) ported from published MATLAB code (Harrison et al, 2015).

Standard IV curve

To calculate neuronal resistance, the maximum voltage deflection to the -100 pA current step (before the sag, arrow on Fig 2A) was measured (peak neuronal resistance). The position for the voltage measurement was determined on the voltage traces at time zero (where there was a clear peak), and then the same position was used for the rest of the voltage traces at subsequent time points.

Dynamic IV curve

As well as measuring the static properties of the neuron at rest it is also useful to measure the effective parameters when the neuronal voltage is subject to a fluctuating drive, as is the case in-vivo. To this end we employed the dynamic IV-curve protocol (Badel et al, 2008) in which a stochastic current I_{inj} in injected into the cell to induce a fluctuating voltage response and triggering of action potentials (Fig 2B). A detailed description of the protocol has been previously published (Badel et al, 2008) as well as the computer code required (Harrison et al, 2015). In brief, a noisy current trace I_{inj} is generated computationally (from the sum of two Ornstein-Uhlenbeck gaussian processes with time constants τ_{fast} = 3 ms and τ_{slow} = 10 ms to mimic AMPA and $GABA_A$ receptor time courses) and injected into the cell with the resultant voltage measured. The voltage equation 1 can be re-arranged for the ionic current to give

$$I_{ion} = I_{inj} - C\frac{dV}{dt} \qquad \text{Eq 3}$$

where the injected current is known, and the derivative can be calculated from measured voltage (with the capacitance extracted using the method in Badel et al, 2008). The ionic current and voltage time courses can then be plotted against each other (see Fig. 2C, red scattered points). Given the interaction of the gated ionic currents with the stochastic injected current, there is significant scatter in the relation. However, the ionic current can be averaged in voltage slices to provide the dynamic IV-curve (see Fig 2C, black solid line and expanded view in Fig 2D). Once the dynamic IV-curve has been obtained the various features can be extracted such as the ohmic conductance - the linear component of the IV-curve at more hyperpolarised subthreshold voltage - and the excess depolarisation-activated current seen in these cells near threshold.

By using both DIV and SIV we use two independent methods that induce distinct voltage dynamics to extract neuronal parameters thereby increasing the robustness of the data. These approaches also examine the neurons under different conditions. For SIV, the parameters are extracted from neurons that are in a simple dynamical state. In contrast the fluctuations induced by the DIV protocol result in a voltage that rapidly explores a much larger range.

Results

Characterising dopaminergic neurons in the substantia nigra

Whole-cell patch-clamp recordings were made from putative dopaminergic neurons located in the SNpc (identified by position in the slice). Neurons were initially confirmed to be SNpc dopaminergic neurons from their electrophysiological profile, which was consistent with previous studies (Grace and Onn, 1989; Richards et al 1997; Krashia et al 2017). Most of the recorded neurons displayed slow autonomous firing (36 out of 49 neurons, 73 %, mean firing rate of 1.05 ± 0.082 Hz Fig 1A) consistent with the reported properties for dopamine neurons in the SNpc (Grace and Onn, 1989). These neurons were sensitive to dopamine (Lacey et al 1989), with application of dopamine (30 μM) hyperpolarising the membrane potential by 7.35 ± 1.24 mV and abolishing the spontaneous firing (Fig 1A, n = 8). The neurons showed a characteristic (Neuhoff et al, 2002) response to step-current injection (Fig 1B), with a large sag in response to hyperpolarising current steps (Fig 1C) indicative of the presence of I(h). Following the termination of hyperpolarising-current steps there was a rebound potential leading to firing in 33 out of 49 neurons (68 %, Fig 1C) another characteristic of I(h). Dopamine reduced the firing in response to the positive current steps and to the naturalistic current injection (firing rate reduced to 62.7 ± 0.2 % of that in control). Dopamine also reduced the voltage response to hyperpolarising current steps (indicative of an increase in whole-cell conductance) and also abolished the rebound firing (Fig 1D). Application of ZD7288 (100 μM), a pharmacological inhibitor of I(h) in dopamine neurons (Harris and Constanti, 1995) greatly reduced the sag response produced by hyperpolarising current steps and also abolished the rebound firing, confirming that they were I(h) mediated (Fig 1E, *n* = 6). Finally, to confirm that the neurons were dopaminergic, a subset of the recorded neurons (*n* = 9) were filled with AF594 dye via the patch pipette and immunofluorescence staining was used to confirm that they were tyrosine hydroxylase positive (Fig 1F).

Detailed analysis of the electrophysiology of dopaminergic neurons in the substantia nigra

We used two approaches to characterise changes that occurred when SNpc dopaminergic neurons had either α-syn aggregates, monomers or vehicle introduced. The first constituted of measurements from standard IV-curve protocols during which neurons received constant-current (step) inputs (Fig. 2A). The second approach measures neuronal properties using the dynamic IV-curve protocol (Badel et al, 2008a, 2008b; Harrison et al, 2015) during which neurons were stimulated by a stochastic current mimicking fluctuating synaptic drive (Fig 2B-D). This methodology allows for the average ionic current at a particular voltage to be measured at a good resolution over the full voltage range. The resulting dynamic IV-curve can be used to provide capacitance, ohmic conductance at hyperpolarised regimes as well as the strength of excess current seen near threshold in these cells (see Fig. 2B-D). It is clear that the dynamic IV curve diverges from linear at potentials above ~ -50 mV (but below action-potential threshold) which is characteristic of a depolarisation-activated outward current (Fig 2D). This effect of the outward current can be isolated by subtracting an extrapolated fit to the linear portion of the dynamic IV curve (as illustrated in the inset to Fig 2D).

Characterising the structure of the alpha synuclein (α-syn) aggregates

Recombinant human alpha-synuclein protein was purchased from Abcam in the form of pre-formed fibril aggregates (PFFs; ab218819) and in the form of monomers (ab218818). Negative stain- transmission electron microscopy (TEM) was initially to confirm that the samples were either monomeric (Fig 3B) or PFFs (Fig 3C). To enable delivery of aggregates, mostly in oligomeric form, via the patch pipette, the PFFs were broken down. We used sonication (as in Polinski et al, 2018) for 15 minutes (50-60 Hz). We compared the structure of the α-syn aggregates (sonicated PFFs) to oligomeric tau which had an annular structure (Fig 3A, Hill et al 2019) to ensure that it consisted of oligomeric species (Fig 3B). These oligomeric forms were stable for at least 3 hours on ice. While the majority of the species in our samples had an oligomeric structure, we cannot exclude the possibility that other forms of aggregates exist (for example small ~50 nm fibrils; Polinski et al, 2018). We therefore use the term aggregates rather than oligomers. Monomeric or aggregated α-syn samples were introduced into dopaminergic neurons via the patch pipette.

Alpha-synuclein aggregates but not monomers have marked effects on the electrophysiological properties of SN dopaminergic neurons.

We introduced either aggregated or monomeric alpha synuclein (500 nM, same concentration as Kaufman et al, 2016) via the patch pipette during whole-cell current-clamp recording from identified SNpc DNs. To ensure consistency, all molar concentrations were based on the molar mass of monomeric alpha-synuclein as the samples probably contain a range of aggregate sizes (see above). Electrophysiological parameters were then measured from the voltage responses to step currents (standard IV, SIV) and naturalistic current injections (dynamic IV, DIV). The currents for SIV and DIV were injected at 8-minute intervals for the duration of recordings (32 minutes; Kaufmann et al, 2016). In control experiments, the same volume of vehicle (2 μl PBS) was added to the intracellular solution. Recordings (α-syn aggregates, monomers or vehicle) were made from SNpc dopaminergic neurons in interleaved slices to minimise variation.

At time zero (a few minutes following whole-cell breakthrough) there was no significant difference in the measured parameters from SIVs (membrane potential P = 0.4657, resistance P = 0.2747 and firing rate P = 0.8511, Table 1) between neurons which had received either vehicle, α-syn monomers or aggregates. Thus, the recording quality and neuronal properties were comparable between the experimental groups. However, as illustrated in the example in Fig 4A, there were marked changes in the SIV during recording from neurons in which α-syn aggregates had been introduced. The changes in SIV, reduction in voltage responses and decrease in firing rate at positive potentials, were indicative of a significant fall in neuronal resistance and the opening of a membrane channel. Such large changes in the SIV did not occur in the neurons that received either α-syn monomers or vehicle (Fig 4B, C). For the neurons injected with α-syn aggregates, after 32 minutes of recording, the resistance was significantly ($p = 0.0029$, $n = 11$) reduced to 63 ± 9.21 % of the resistance measured at 0 mins (Fig 4D). There was no significant changes in the resistance for neurons injected with either α-syn monomers ($P = 0.4688$, $n = 6$) or vehicle ($P = 0.0645$, $n = 10$) over the duration of recordings (at 32 mins IR was 94 ± 5% of the resistance measured at time 0 mins for vehicle and 99 ± 9 % of resistance measured at time 0 mins for monomers, Fig 4D). At the 32-minute time point there was a significant ($P = 0.0007$) difference in resistance between the neurons that received α-syn monomers or vehicle to those where α-syn aggregates were introduced. We investigated the time at which α-syn aggregates began to affect neuronal resistance and found that the difference in resistance between control and aggregated and monomeric α-syn neurons first became significant at the 16 minute time point ($p = 0.0048$; Figure 4D). Thus, the resistance started to fall (presumably as membrane channels opened) between 8 to 16 minutes after α-syn aggregate introduction into the neuron at whole-cell break through.

The recorded neurons had a membrane potential of around -55 mV (see Table 1 supplementary data) at the start of recordings. For all experimental conditions, the membrane potential slowly and weakly depolarised over the duration of the recordings (Fig

4E). For vehicle, the mean depolarisation (ΔVm) was 6.2 ± 1.82 mV after 32 minutes of recording (P = 0.0234, *n* = 10), for α-syn monomers ΔVm was 3.8 ± 1.2 mV (P = 0.0938, *n* = 6) and for α-syn aggregates ΔVm was 6.8 ± 1.85 mV (P = 0.0107, *n* = 11). There was no statistically significant difference between the membrane potentials of the control (vehicle and monomers) vs α-syn aggregates across the duration of the recordings (P = 0.3273). Thus although α-syn aggregates markedly reduced neuronal resistance they did not produce a significant change in the membrane potential.

For control neurons (vehicle), although the membrane potential was depolarised, the change in firing rate did not reach significance (P = 0.1895, measured from the naturalistic current injection, firing rate at 32 mins was 124.7 ± 1.3 % of the firing rate at time 0 mins, *n* = 10, Fig 4F, G). For neurons which received α-syn monomers, although the membrane potential was depolarised there was also no significant (P > 0.9999) change in the firing rate (measured from the naturalistic current injection, firing rate at 32 mins was 120.4 ± 2.4 % of the firing rate at time 0 mins, *n* = 6, Fig 4F, G). For the neurons which had α-syn aggregates introduced, there was a significant (P = 0.0020) reduction in the firing rate (at 32 mins the firing rate was 42.3 ± 9.3 % of the firing rate measured at 0 mins, *n* = 11, Fig 4F, G). When comparing control (vehicle and monomers) vs α-syn aggregates there was a significant difference in the firing rate at 32 minutes (P = 0.0061). This fall in firing rate induced by α-syn aggregates is consistent with the marked fall in neuronal resistance.

Alpha-synuclein aggregates decreased the occurrence of rebound firing following the termination of hyperpolarisation steps (73 % of neurons (8/11) showed rebound firing at 0 mins, but only 18 % (2/11) till showed it after 32 minutes of recording). In contrast, all the control neurons that initially displayed rebound firing (60 %, (6/10)) still showed it after 32 minutes of recording. Aggregated α-syn also reduced the occurrence of tonic firing (64 % of neurons (7/11) were initially spontaneously active but after 32 minutes only 27 % (3/11) of neurons were still active). For control neurons, 80 % (8/10) initially displayed tonic firing, with 60 % (6/10) still active after 32 minutes of recording. We examined at what time the neurons stopped spontaneously firing and found that on average control (vehicle) neurons that ceased firing stopped firing at 26 ± 3.7 minutes, which was similar to the time for neurons that received α-syn monomers (28 ± 3.64 minutes). The neurons that received α-syn aggregates stopped firing significantly earlier (15.1 ± 2.33 minutes) than either control (vehicle) neurons ($P = 0.0274$) or neurons that received α-syn monomers ($P = 0.0392$).

Further analysis of the effects of α-syn aggregates on dopaminergic neurons using the dynamic IV curve

In control neurons (vehicle) the DIV curve did not markedly change throughout the duration of recordings (Fig 5A). In contrast α-syn aggregates induced significant changes to the DIV, in particular increasing the slope (Fig 5B). These effects were not observed with α-syn monomers (Fig 5C). For all experimental conditions, there were no significant changes in the cellular capacitance ($P = 0.18$, Fig 5E). Thus, the introduction of α-syn aggregates had no effect on the electrotonic properties of the neurons, by for example electrically isolating compartments. Aggregated α-syn markedly increased the membrane conductance (272 % of the conductance at 0 mins by 32 minutes, $P = 0.001$, Fig 5D). In control neurons (vehicle or α-syn monomers) there was a small increase in conductance (vehicle conductance was 135 % of the conductance at 0 mins by 32 minutes $P = 0.009$; α-syn monomer conductance was 141.2 % of the conductance at 0 mins by 32 minutes, ns) over the duration of recordings. At 32 minutes there was no significant ($P > 0.9999$) difference between the conductance of vehicle and α-syn monomer treated neurons. In contrast, the conductance of α-syn aggregate treated neurons was significantly ($P = 0.0003$) larger than vehicle treated neurons. There was no significant differences in the other extracted parameters: resting membrane potential, spike potential or spike-resting potential between the 3 experimental conditions (Fig 5F-H). Thus the reduction in excitability induced by α-syn aggregates is only due to a change in conductance rather than changes in for example the potential difference between rest and threshold.

The decrease in conductance and firing rate caused by alpha synuclein is in part due to the opening of KATP channels

Previous studies have shown that either blocking ATP-sensitive K channels (KATP) or genetically deleting them it has protective effects on dopaminergic neurons in PD rodent models (Liss et al 2005; Zhang et al 2012). There has also been a recent preprint that shows that the effects of α-syn aggregates on spontaneous firing can be prevented by blocking KATP channels (Thakur et al, 2019). To investigate whether the increase in membrane conductance that we have observed could be prevented by inhibiting KATP channel opening, we used the classic KATP blocker glibenclamide (Light and French 1994; Jiang and Haddad 1997). We first investigated whether the presence of glibenclamide throughout recordings had any effect on the electrophysiological properties of SNpc dopaminergic neurons (Fig 6A). There was no significant difference in any of the measured parameters (from SIVs, membrane potential P = 0.3791, resistance P = 0.2294, firing rate P = 0.6548) at 0 mins between neurons from slices which had been pre-incubated with glibenclamide (1 μM, *n* = 6) compared to neurons in control slices (both with vehicle in the patch pipette). These neuronal parameters did not significantly change over the duration of the recordings with glibenclamide present: resistance (after 32 mins 99 ± 7.5 % of the resistance at time 0 mins, P = 0.08438, *n* = 6) or firing rate (after 32 mins 112.1 ± 26.6 % of the firing rate at time 0 mins, P = 0.5625, Fig 6A). Thus, glibenclamide had no significant effect on neuronal properties measured from SIVs that could occlude the actions of α-syn aggregates.

We then made whole-cell recordings with α-syn aggregates in the patch pipette in slices pre-incubated in glibenclamide (1 μM, Fig 6B). The fall in resistance and firing rate that was observed in the presence of α-syn aggregates did not occur when the slices were incubated with glibenclamide. There was no significant reduction in resistance or firing rate over the duration of recording when slices were incubated with glibenclamide suggesting that the action of α-syn aggregates could least in part be mediated by KATP channels. The resistance at 32 mins was 90 ± 8.62 % of the resistance at time 0 mins (cf 63 % without glibenclamide) which was not statistically significant (P = 0.25, *n* = 6) from the resistance at time zero. The firing rate was 80.14 ± 12.89 % of the rate at time 0 mins (vs 42 % without glibenclamide) which was not statistically significant from the firing rate at time 0 mins (P = 0.353, *n* = 6). Both sets of recorded neurons (vehicle and α-syn aggregates) weakly depolarised over the 32 minutes of recording to a similar degree to that of non-glibenclamide treated slices (vehicle, ΔVm 4.66 ± 2.6 mV and α-syn aggregates, ΔVm 5.5 ± 2.05 mV, Fig 6E).

We further investigated the effects of the glibenclamide on the effects of α-syn aggregates - using the dynamic IV (DIV). The DIV curves in glibenclamide (vehicle) and in glibenclamide (α-syn aggregates) did not markedly change throughout the duration of the recordings (Fig 7A, B). As observed previously (without glibenclamide) there was also no change in capacitance over the duration of the recordings ((vehicle P = 0.0625, α-syn aggregates P = 0.0625, Fig 7C). In the presence of glibenclamide, there was no significant increase (P = 0.0625) in whole cell conductance for vehicle receiving neurons over the duration of the recordings or only a small increase for α-syn aggregate receiving neurons (P = 0.0313). After 32 minutes, there was no significant (P = 0.3095) difference between the whole cell conductance of neurons receiving vehicle and those receiving α-syn aggregates (Fig 7D, H). For all the other extracted parameters there was no difference between vehicle and α-syn aggregate receiving neurons for the duration of recordings (Fig 7E-G). Thus, as observed with SIV anlysis, the KATP inhibitor glibenclamide significantly reduced the effects of α-syn aggregates.

Discussion

In this study we have used whole-cell patch-clamp recording to introduce a known concentration and form of aggregated alpha synuclein (α-syn) into single substantia nigra pars compacta (SNpc) dopaminergic neurons in acutely isolated mouse slices. Although it is possible, using emerging technologies, to isolate only the oligomeric fractions (Kumar et al, 2020) we have not utilised such methods. Thus we cannot exclude the possibility that some small fibrils are present in our α-syn oligomer samples. While the majority of the species in our α-syn samples appeared to have an oligomeric structure (Fig 3) other forms of small aggregates maybe present (for example small ~50 nm fibrils; Polinski et al, 2018). We have therefore used the term α-syn aggregates rather than α-syn oligomers. As outlined in previous studies (Kaufmann et al 2016; Hill et al 2019) delivery of species via the patch pipette has a number of advantages, the main one being that it is possible to measure early changes in the properties of a single neuron in a network that is free from pathology. This method also bypasses any slow uptake steps and each neuron acts as its own control, as at early time points only low concentrations of the species will have diffused into the neuron. Here we have introduced 500 nM of α-syn aggregates, which is a concentration in line with previous studies (see Kaufmann et al, 2016). However, as noted in the methods, the actual concentration of aggregates will be considerably lower. It would be interesting in future experiments to investigate whether there is a concentration dependant effect of α-syn aggregates, with for example lower concentrations having a slower onset (see Hill et al 2019).

We used both standard current-voltage relationships (SIV, with step current injections) and the dynamic current-voltage relationships (DIV, with naturalistic current injection) to extract neuronal parameters. Both approaches measured a marked increase in whole-cell conductance (fall in neuronal resistance), which occurred between 8-16 minutes after whole-cell break through. There were no significant changes in membrane potential, cell capacitance or spike threshold between neurons receiving α-syn aggregates, α-syn monomers or vehicle. The increase in conductance significantly reduced the firing rate, both induced (by current injection) and spontaneous, and abolished rebound firing following hyperpolarising current steps. The increase in conductance increased the linearity of the DIV curve effectively shunting the depolarisation-activated conductance increase just below threshold that was present in some neurons at 0 minutes (whole-cell breakthrough).

Obtaining similar results using two independent methods for the extraction of neuronal parameters strengthens the robustness of the observation that α-syn aggregates increase whole-cell conductance. There were minor differences in the precise values of the neuronal parameters extracted using DIV compared to those extracted with SIV, which is to be expected given the different conductance states of the cell in the two protocols. For the DIV, the voltage varies across a wide range during naturalistic stimulation (mimicking in vivo synaptic activity) activating and inactivating a variety of conductances. In contrast the SIV extracts parameters over a much smaller range of voltages from essentially quiescent cells. For example, if the DIV and SIV curves are compared, the DIV conductances are initially lower (at 0 minutes) for all of the experimental conditions (vehicle, aggregates and monomers) and then increase. This could be interpreted as one or more of the conductances being slightly more inactivated during the DIV protocol. It could then be that this inactivation is relieved as the neuronal resting potential slowly depolarises during the recording. Alternatively, it could be that another conductance activates as the neuron depolarises, but in a range that is not accessed by the hyperpolarising SIV current steps. In either case, a different range of voltages is probed between DIV and SIV and so differences in the extracted parameters will occur. The fact that the same significant conductance increase (resistance decrease) is clearly seen in these two very different protocols attests to the robustness of the effect of alpha-synuclein on these neurons.

The increase in whole-cell conductance is reduced by the KATP channel blocker glibenclamide

The effects of the ATP-sensitive K^+ channel (KATP) inhibitor glibenclamide (Light and French 1994) suggests the involvement of KATP channels (but see caveats below). KATP channels are inwardly rectifying K^+-selective ion channels that are inhibited by intracellular ATP. KATP channels provide a link between the energy state of cells and their electrical activity acting as a metabolically controlled "brake on excitation". A decrease in sub-membrane ATP levels and an accompanying rise in ADP concentration (during activity) triggers KATP channel opening dropping neuronal resistance and hyperpolarising the membrane potential (Stanford and Lacey 1995; Seino, 1999; Haller et al., 2001). It is well established that SNpc dopaminergic neurons express KATP channels (Schiemann et al 2012; Liss et al 2005). The lack of effect of the KATP inhibitor glibenclamide under control conditions suggests that few KATP channels are open at rest. This is perhaps not surprising as there was 2 mM ATP in the intracellular patch solution, although some KATP channels have a low affinity for ATP and would still be open with this level of ATP (for example see Allen and Brown 2004). The effects of α-syn aggregates on conductance and its inhibition by glibenclamide are consistent with the opening of KATP channels (but see below). These effects occurred in the presence of 2 mM intracellular ATP suggesting a direct effect of α-syn aggregates on the KATP channel, rather than via a reduction in intracellular ATP concentration (by for example mitochondrial dysfunction). KATP channel openers like diazoxide have previously been shown to act by open KATP channels in the presence of ATP (Schwanstecher et al 1998) so it is possible that α-syn aggregates could have a similar action.

The effects on cell conductance and its prevention with glibenclamide are consistent with the α-syn aggregates increasing KATP channel open probability. However, there was little or no associated membrane potential hyperpolarisation (measured with SIV and with DIV), which has been observed in most reports of KATP channel activation (for example see Stanford and Lacey, 1995; Allen and Brown 2004). The equilibrium potential for K^+ is ~ -95 mV, so opening of KATP channels would be expected to produce a large hyperpolarisation of the membrane potential (as the resting potential at time zero was ~-55 mV). However, the membrane potential hyperpolarisation could possibly be counteracted by the opposing activation of hyperpolarization-activated, cyclic nucleotide-gated HCN channels I(h) which have a reversal potential between -40 to -30 mV (Mayer and Westbrook 1983). It may be that the opening of a relatively small number of KATP channels changes the input resistance/conductance of neurons but is insufficient to change the membrane potential against the responsive reaction of I(h). In contrast opening of many KATP channels will overcome the effects of I(h) leading to robust membrane hyperpolarisation, which as reported for SNpc dopaminergic neurons by lowering intracellular ATP concentration or using KATP channel opening drugs (Stanford and Lacey 1995).

The inhibitory effects of glibenclamide on α-syn responses are consistent with the opening of KATP channels but additional evidence is required to provide definitive evidence for a role for KATP channels in the effects of α-syn aggregates. One possible approach is to occlude the effects of α-syn aggregates using a pharmacological opener of KATP channels (such as diazoxide). However these experiments maybe be difficult to interpret. The KATP channel opener will markedly reduce resistance and hyperpolarise the recorded neuron. This may occlude the effects of α-syn aggregates simply by shunting the neuron and moving it closer to E_K rather than acting through the same channel. Other possible approaches include the use of transgenic animals, where the KATP gene has been deleted, or using cell lines expressing specific KATP channels. Alternate possibilities for the lack of membrane hyperpolarisation include the opening of other channels that depolarise the neuron. For example, it has been reported that α-synuclein itself can form non-selective cation channels (Mironov et al, 2015).

It took on average between 8-16 minutes of dialysis for the effects of α–syn aggregates on whole cell conductance to become significant. It may be that the concentration within the neuron has to reach a sufficient level to open membrane channels. For comparison introduction of aggregated tau (444 nM) into pyramidal neurons started to have effects on the action potential within the first 10 minutes (Hill et al, 2019). In this study we chose to focus on the effects of introducing α-syn aggregates into substantia nigra dopaminergic neurons. Given that the neighbouring population of VTA dopaminergic neurons have differences in their KATP channel expression (Liss et al, 2005), it might be expected that α-syn aggregates may have a different effect in these cells (which would additional evidence for a role of KATP channels). This may contribute to the varying vulnerability of these two dopaminergic nuclei in diseases like Parkinson's disease.

The accumulation of α-syn aggregates in SN dopaminergic neurons during Parkinson's disease progression could potentially result in the prolonged activation of membrane channels (such as KATP) which will chronically reduce electrical activity, the amount of dopamine released (Patel et al, 2011) and will be detrimental to neuron function. If KATP channels are involved then there will be a loss of the metabolic feedback mechanism. Consistent with this KATP involvement, there is retrospective epidemiological evidence of a reduced risk for Parkinson's disease in type 2 diabetic patients that were treated with KATP inhibitors (Schernhammer *et al*, 2011; Wahlqvist *et al,* 2012; Cereda *et al*, 2013; Lu *et al,* 2014; Brauer *et al*, 2015).

Conclusion

In this study we have combined electrophysiological recording with detailed and thorough analysis to characterize the effects of introducing aggregated α-Syn directly into single mouse dopaminergic neurons in the substantia nigra. Aggregated α-Syn caused a significant increase in conductance and decrease in firing rate without altering the resting membrane potential, capacitance or spike threshold. Changes to conductance and firing rate occurred

8-16 minutes after whole-cell breakthrough and were specific to aggregates (they were not observed when monomeric alpha synuclein was introduced). The effects could be prevented by pre-incubating the slices in ATP-sensitive potassium channel (KATP) inhibitor glibenclamide, despite the high concentration of ATP present in the patch electrode. This suggests that aggregated α-Syn may increasing the opening probability of K_{ATP} channels, resulting in an increase in conductance, a reduction in neuronal excitability and likely also a decrease in dopamine release and overall cell function.

References

Alderson TR, Markley JL (2013) Biophysical characterization of α-synuclein and its controversial structure. *Intrinsically Disord Proteins*. 1(1):18-39.

Allen TG, Brown DA. (2004) Modulation of the excitability of cholinergic basal forebrain neurones by KATP channels. J Physiol. 554(Pt 2):353-70.

Badel L, Lefort S, Brette R, Petersen C, Gerstner W, Richardson, M (2008a). Dynamic I-V Curves Are Reliable Predictors of Naturalistic Pyramidal-Neuron Voltage Traces. *Journal of Neurophysiology,* 99(2): 656-666.

Badel L, Lefort S, Berger T, Petersen C, Gerstner, W, Richardson, M (2008b). Extracting non-linear integrate-and-fire models from experimental data using dynamic I–V curves. *Biological Cybernetics*, 99(4-5): 361-370.

Bernheimer H, Birkmayer W, Hornykiewicz O, Jellinger K, Seitelberger F (1973) Brain dopamine and the syndromes of Parkinson and Huntington. Clinical, morphological and neurochemical correlations. *Journal of the Neurological Sciences*. 20(4):415–455

Bengoa-Vergniory, N., Roberts, R., Wade-Martins, R. and Alegre-Abarrategui, J., 2017. Alpha-synuclein oligomers: a new hope. Acta Neuropathologica, 134(6), pp.819-838.

Bezanson J, Edelman A, Karpinski S, Shah VB (2014) Julia: A fresh approach to numerical computing. *SIAM review*. ;59(1):65–98.

Brauer R, Bhaskaran K, Chaturvedi N, Dexter DT, Smeeth L., Douglas I (2015) Glitazone Treatment and Incidence of Parkinson's Disease among People with Diabetes: A Retrospective Cohort Study. *PLoS Med* 12(7):e1001854.

Burre J, Sharma M, Tsetsenis T, Buchman V, Etherton MR, Suedhof TC (2010) alpha Synuclein Promotes SNARE-Complex Assembly in Vivo and in Vitro. *Science* 329:1663-1667.

Cereda E, Barichella M, Pedrolli C, Klersy C, Cassani E, Caccialanza R, Pezzoli G. (2012) Diabetes and risk of Parkinson's disease. *Mov Disord*. 28(2):257

Damier P, Hirsch EC, Agid Y, Graybiel AM (1999) The substantia nigra of the human brain. II. Patterns of loss of dopamine-containing neurons in Parkinson's disease. *Brain.* 122:1437-1448.

Grace AA, Onn SP (1989) Morphology and electrophysiological properties of immunocytochemically identified rat dopamine neurons recorded in vitro. *J Neurosci* (10):3463-81.

Haller M, Mironov SL, Karschin A, Richter DW (2001) Dynamic activation of K(ATP) channels in rhythmically active neurons. *J Physiol.* 537(Pt 1):69-75

Harris NC, Constanti A (1995) Mechanism of block by ZD 7288 of the hyperpolarization-activated inward rectifying current in guinea pig substantia nigra neurons in vitro. *J Neurophysiol.* 74(6):2366-78.

Harris N, Webb C, Greenfield S, (1989) A possible pacemaker mechanism in pars compacta neurons of the guinea-pig substantia nigra revealed by various ion channel blocking agents. *Neuroscience* 31(2): 355-362.

Harrison PM, Badel L, Wall MJ and Richardson MJE (2015) Experimentally verified parameter sets for modelling heterogeneous neocortical pyramidal-cell populations *PLOS Computational Biol* 11: e1004165

He C, Chen F, Li B, Hu Z (2014) Neurophysiology of HCN channels: from cellular functions to multiple regulations. *Prog Neurobiol* 112:1-23.

Hill E, Karikari TK, Moffat G, Richardson MJE, Wall MJ (2019) Introduction of tau oligomers into cortical neurons alters action potential dynamics and disrupts synaptic transmission and plasticity. eNeuro .0166-19.2019,

Iwai A, Masliah E, Yoshimoto M, Ge N, Flanagan L, de Silva HA, Kittel A, Saitoh T (1995) The precursor protein of non-A beta component of Alzheimer's disease amyloid is a presynaptic protein of the central nervous system. *Neuron*. 14(2):467-75.

Jakes R, Spillantini MG, Goedert M (1994) Identification of 2 distinct synucleins from human brain. FEBS Letters 345:27-32.

Kaufmann TJ, Harrison P, Richardson MJE, Pinheiro TJT, Wall MJ (2016) Intracellular injection of soluble alpha synuclein oligomers reduces pyramidal cell input resistance and firing rate. *J Physiol* 594 (10): 2751-2772

Kumar, S. T., Donzelli, S., Chiki, A., Syed, M. M. K., & Lashuel, H. A. (2020). A simple, versatile and robust centrifugation-based filtration protocol for the isolation and quantification of α-synuclein monomers, oligomers and fibrils: Towards improving experimental reproducibility in α-synuclein research. Journal of Neurochemistry.

Jiang C, Haddad GG (1997) Modulation of K+ channels by intracellular ATP in human neocortical neurons. *J Neurophysiol*. 77(1):93-102.

Krashia P, Martini A, Nobili A, Aversa D, D'Amelio M, Berretta N, Guatteo E, Mercuri NB. (2017) On the properties of identified dopaminergic neurons in the mouse substantia nigra and ventral tegmental area. *Eur J Neurosci* .45(1):92-105.

Lacey MG, Mercuri NB, North RA (1989) Two cell types in rat substantia nigra zona compacta distinguished by membrane properties and the actions of dopamine and opioids. *J Neurosci*. 9(4):1233-41.

Lashuel HA, Overk CR, Oueslati A, Masliah E (2013) The many faces of alpha synuclein: from structure and toxicity to therapeutic target. *Nature Reviews Neuroscience* 14:38-48

Light PE, French RJ (1994) Glibenclamide selectively blocks ATP-sensitive K+ channels reconstituted from skeletal muscle. *Eur J Pharmacol* 259(3):219-22.

Liss B, Haeckel O., Wildmann J., Miki T., Seino S., Roper J. (2005) K-ATP channels promote the differential degeneration of dopaminergic midbrain neurons. *Nature Neurosci* 8(12):1742-51.

Lu L, Fu DL, Li HQ, Liu AJ, Li JH, Zheng GQ. (2014) Diabetes and risk of Parkinson's disease: an updated meta-analysis of case-control studies. *PLoS One*. 21;9(1):e85781.

Mahul-Mellier, A., Burtscher, J., Maharjan, N., Weerens, L., Croisier, M., Kuttler, F., Leleu, M., Knott, G. and Lashuel, H., 2019. The process of Lewy body formation, rather than simply alpha-synuclein fibrillization, is the major driver of neurodegeneration in synucleinopathies.

Mayer M.L., Westbrook G.L. 1983. A voltage-clamp analysis of inward (anomalous) rectification in mouse spinal sensory ganglion neurones. J. Physiol. 340:19–45

Michel PP, Hirsch EC, Hunot S (2016) Understanding Dopaminergic Cell Death Pathways in Parkinson Disease. *Neuron.* 90(4):675-91.

Mironov S (2015) α-Synuclein forms non-selective cation channels and stimulates ATP-sensitive potassium channels in hippocampal neurons. *J Physiol* 593(1):145-59.

Murphy DD, Rueter SM, Trojanowski JQ, Lee VMY (2000) Synucleins are developmentally expressed, and alpha-synuclein regulates the size of the presynaptic vesicular pool in primary hippocampal neurons. *Journal of Neurosci* 20:3214-3220.

Neuhoff H, Neu A, Liss B, Roeper J (2002) I(h) channels contribute to the different functional properties of identified dopaminergic subpopulations in the midbrain. *J Neurosci.* 22(4):1290-302

Patel JC, Witkovsky P, Coetzee WA, Rice ME (2011) Subsecond regulation of striatal dopamine release by pre-synaptic KATP channels. *J Neurochem*. 118(5):721-36

Polinski NK, Volpicelli-Daley LA, Sortwell CE, Luk KC, Cremades N, Gottler LM, Froula J, Duffy MF, Lee VMY, Martinez TN, Dave KD (2018) Best Practices for Generating and Using Alpha-Synuclein Pre-Formed Fibrils to Model Parkinson's Disease in Rodents. *J Parkinson's Dis*. 8(2):303-322.

Richards CD, Shiroyama T, Kitai ST. (1997) Electrophysiological and immunocytochemical characterization of GABA and dopamine neurons in the substantia nigra of the rat. *Neuroscience.* 80(2):545-57.

Schernhammer E, Hansen J, Rugbjerg K, Wermuth L, Ritz B. Diabetes and the risk of developing Parkinson's disease in Denmark. *Diabetes Care* 34(5):1102-8.

Schiemann J, Schlaudraff F, Klose, V, Bingmer M, Seino S, Magill P, Zaghloul KA, Schneider G, Liss B, Roeper J (2012) K-ATP channels in dopamine substantia nigra neurons control bursting and novelty-induced exploration *Nat Neurosci* .15(9):1272-80.

Schwanstecher M, Sieverding C, Dorschner H, et al. (1998) Potassium channel openers require ATP to bind to and act through sulfonylurea receptors. *EMBO J.* 1998;17(19):5529–5535

Seino S (1999) ATP-sensitive potassium channels: a model of heteromultimeric potassium channel/receptor assemblies. *Annu Rev Physiol*. 61:337-62.

Spillantini MG, Schmidt ML, Lee VMY, Trojanowski JQ, Jakes R, Goedert M (1997) α-Synuclein in Lewy bodies. Nature. 388:839–840.

Stanford IM, Lacey MG (1995) Regulation of a potassium conductance in rat midbrain dopamine neurons by intracellular adenosine triphosphate (ATP) and the sulfonylureas tolbutamide and glibenclamide. *J Neurosci*. 15(6):4651-7.

Thakur P, Luk K, Roeper J (2019). Selective K-ATP channel-dependent loss of pacemaking in vulnerable nigrostriatal dopamine neurons by α-synuclein aggregates. [*preprint* doi: https://doi.org/10.1101/842344]

Wahlqvist M, Lee MS, Hsu CC, Chuang SY, Lee Jy, Tsai HN (2012) Metformin-inclusive sulfonylurea therapy reduces the risk of Parkinson's disease occurring with Type 2 diabetes in a Taiwanese population cohort. *Parkinsonism Relat Disord* 18(6):753-8.

Winner B, Jappelli R, Maji SK, Desplats PA, Boyer L, Aigner S, Hetzer C, Loher T, Vilar M, Campioni S (2011) In vivo demonstration that α-synuclein oligomers are toxic. Proc. Natl. Acad. Sci. USA. 108:4194–4199.

Zhang Q, Li C, Zhang T, Ge Y, Han X, Sun S, Ding J, Lu M, Hu G (2018) Deletion of Kir6.2/SUR1 potassium channels rescues diminishing of DA neurons via decreasing iron accumulation in PD. *Mol Cell Neurosci*. 164-176.

Legends

Figure 1: Whole-cell patch-clamp recording from dopaminergic neurons in the SNpc

(A) Example membrane potential trace recorded from a putative dopaminergic neuron (DN) in the substantia nigra which showed characteristic spontaneous action potential firing. Dopamine (30 μM) hyperpolarised the neuron from -62 mV to -70 mV and stopped the action potential firing. (B) The different input currents delivered to putative DNs. SIV is the standard step current protocol, 3 s duration steps starting at -200 pA and increasing by 50 pA until the neuron exhibits a regular firing pattern. DIV uses a fluctuating naturalistic noisy current trace (see methods for details) which is also used to determine action potential firing rate. (C) (Top) Membrane potential traces in response to current steps. The recorded neuron displays characteristic features of DNs: a large sag in response to hyperpolarising steps (arrow) and rebound firing (*). (Bottom) Membrane potential trace from the same cell in response to naturalistic current injection. The neuron can be seen to be firing at rest (*) which is a characteristic feature of these neurons. (D) (Top) Membrane potential traces in response to current steps following application of dopamine (30 μM). The sag is reduced, the membrane potential hyperpolarised, the firing reduced, and the rebound firing is absent. (Bottom) Membrane potential trace from the same cell in response to naturalistic current injection in dopamine (30 μM). The neuron has stopped firing at rest, fires less frequently during current application and is hyperpolarised. (E) (Top) Membrane potential traces in response to current steps in the presence of the I(h) blocker ZD7288 (100 μM) are similar to that previously reported for DN (Harris and Constanti, 1995). The sag response to hyperpolarising current steps is markedly reduced, the resting membrane potential is hyperpolarised, the firing rate reduced and the voltage response following the spike is altered. (Bottom) Membrane potential response of the same neuron to the naturalistic injected current in ZD7288 (100 μM). (F) Tyrosine hydroxylase (TH) immunohistochemistry confirms that the recorded neurons were DNs. Neurons were filled with AF594 dye (red) via the patch pipette and then slices were stained for TH (green). The merged image shows that the recorded neurons express tyrosine hydroxylase and are therefore dopaminergic. The scale bar is 50 μm.

Figure 2: Extracting neuronal parameters using standard-IV (SIV, panel A) and dynamic-IV (DIV, panels B-D) methodologies. For the SIV measurements: (A) Applied current and voltage response. Arrow shows location of voltage measurement for the calculation of neuronal resistance (peak voltage deflection). For the dynamic IV measurements: (B) Naturalistic stimulation current and voltage response. (C) The estimated ionic current as a scatter plot against voltage (points). The dynamic-IV curve (black) is the typical ionic current at a particular voltage where data within 200 ms post-spike was not included to avoid the effects of transitory spike-generated currents. (D) The dynamic IV curve (black) and its linear fit to the ohmic component (green, from hyperpolarised voltages

to the resting voltage). Inset, illustrates the isolated outward current. See Methods for further details of the SIV and DIV fitting procedures.

Figure 3: Structural analysis of alpha synuclein samples.

Electron micrographs of negative-stain-TEM analysed protein samples. The sample (5 μl) was applied onto a copper grid and fixed with uranyl acetate. Magnification is 60,000x. (A) Tau aggregates (for reference) showing aggregated form. Inset, higher magnification showing annular form of aggregates (B) Alpha synuclein monomers show no aggregation. Inset, higher magnification showing no structural form (C) Alpha synuclein aggregates display many large fibrils (preformed fibrils PFF). Inset, example of fibrils at higher magnification (D) Alpha synuclein fibrils were added to intracellular patch solution and then sonicated for 15 minutes to form small aggregates. Inset, illustrates the annular form of aggregates. Scale bar = 200 nm.

Figure 4. Alpha-synuclein aggregates induce a time-dependent decline in firing rate and significant fall in neuronal resistance.

Example current-voltage relationships (SIV) for dopaminergic neurons injected with α-syn aggregates (A), vehicle (B) and α-syn monomers (C). Current steps (starting at -200pA and increasing by 50 pA until a regular firing pattern was induced) were used to construct SIVs. Recordings display SIVs at time points between whole cell breakthrough (0 mins) and up to 32 mins. The neuron which had the α-syn aggregates introduced (A) shows a clear reduction in the voltage responses and a fall in the firing rate at positive potentials, whereas the neurons that received either vehicle or α-syn monomers show no significant changes (B, C). (D) Mean neuronal resistance plotted against time for control (vehicle) neurons and neurons that had either α-syn aggregates or monomers introduced. For the neurons injected with α-syn aggregates, after 32 minutes of recording, the resistance was significantly (p =

0.0029) reduced to 63 ± 9.21 % of the resistance measured at 0 mins. At the 32-minute time point there was a significant (P = 0.0002) difference in resistance between the neurons that received α-syn monomers or vehicle to those where α-syn aggregates were introduced. (E) Mean resting membrane potential plotted against time for control (vehicle) neurons and neurons that had either α-syn aggregates or monomers introduced. Under all experimental conditions, the neurons slowly depolarised over the time course of the recording. For vehicle, the mean depolarisation (ΔVm) was 6.2 ± 1.82 mV after 32 minutes of recording (P = 0.0234), for α-syn monomers ΔVm was 3.8 ± 1.2 mV (P = 0.0938) and for α-syn aggregates ΔVm was 6.8 ± 1.85 mV (P = 0.0107). (F) Normalised firing rate plotted against time for control (vehicle) neurons and neurons that had either α-syn aggregates or monomers introduced (firing rate was measured from naturalistic current injection). Data is normalised to the firing rate at time 0 (whole cell break through). Despite depolarising by a comparable amount to the control (vehicle) and monomer introduced neurons, α-syn aggregates induced a significant reduction in the firing rate over time (P=0.0020) consistent with the fall in input resistance. When comparing control (vehicle and α-syn monomers) and α-syn aggregates there was a significant difference in the firing rate at 32 minutes (P = 0.0061). (G) The same section of voltage trace taken during the injection of naturalistic current in example neurons injected with vehicle, α-syn monomers and α-syn aggregates to illustrate the changes in firing pattern over the duration of recordings.

Figure 5. Intracellular diffusion of alpha-synuclein aggregates results in a progressive conductance increase in the dynamic I-V curve.

Example dynamic IV curves (DIV) from neurons that had control (vehicle, A), alpha-synuclein (α-syn) aggregates (B) or monomeric α-syn (C) introduced. Each graph shows the DIV curve at 8 minute time points throughout recordings (32 minutes). There is a marked increase in the gradient of the DIV (conductance) when oligomeric α-syn was introduced. (D-

H) Extracted neuronal parameters averaged across recordings for the time periods during recordings (*n* =1 0 for control, *n* = 11 α-syn aggregates and *n* = 6 α-syn, monomers). Capacitance (D) showed no significant change over time for all the experimental conditions. Though both control (vehicle) and monomeric α-syn neurons showed a small increase in conductance (E) over time (~35% and ~40% after 32 minutes, respectively), the average conductance for the cells receiving α-syn aggregates was almost threefold its initial value by 32 mins (~170 % increase; P=0.009). At 32 minutes there was no significant (P > 0.9999) difference between the conductance of vehicle and α-syn monomer treated neurons. In contrast, the conductance of α-syn aggregate treated neurons was significantly (P = 0.0003) larger than vehicle treated neurons. Though both the resting potential (F) and spike threshold (G) slightly increased with time, the potential difference from resting potential to spike threshold remained constant with time. The decrease in excitability of the cells receiving α-syn aggregates was therefore mediated by a conductance shunt rather than an increase in the relative threshold for spike initiation.

Figure 6. The effects of alpha-synuclein aggregates on electrophysiological properties are reversed by glibenclamide

(A) Standard current-voltage relationship (SIV) for an example control neuron (injected with vehicle) in the presence of the KATP channel inhibitor glibenclamide (1μM). Current steps (starting at -200pA and rising by 50 pA) were injected until a regular firing pattern was induced. SIV traces are displayed at time points between whole cell breakthrough (0 mins) and the end of recording (32 mins). The neuron remained stable for the duration of the recording with little change in the SIV. (B) As in (A), but with α-syn aggregates (500 nM, final concentration) added to the internal recording solution. The decrease in input resistance and firing rate that was observed with α-syn aggregates in control conditions was markedly reduced by the presence of glibenclamide. (C) Mean resistance measurements over time for control (vehicle) vs α-syn aggregates in the presence of glibenclamide. The fall in resistance was reduced compared to that for α-syn aggregate-injected neurons recorded in normal aCSF. (D) Mean resting membrane potential measurements plotted against time for vehicle vs α-syn aggregates in the presence of glibenclamide. (E) Mean firing rate (measured from naturalistic current injection) plotted against time for vehicle vs α-syn aggregates in the presence of glibenclamide. The fall in firing rate was reduced compared to that for α-syn aggregate-injected neurons in normal aCSF. The red dotted line represents the effects observed with the introduction of α-syn aggregates in the absence of glibenclamide, this data is repeated from Figure 4 and is intended to provide a visual reference to demonstrate the partial recovery.

Figure 7. The KATP channel inhibitor glibenclamide blunts the effects of α-syn aggregates on the DIV.

Slices were incubated in glibenclamide (1 μM) to block KATP channels. (A) Example dynamic IV curves for a neuron that had vehicle introduced. (B) Example dynamic IV curves for a neuron that had α-syn aggregates introduced. For (A and B) each graph shows the DIV curves at 8 minute time points throughout recordings (32 minutes). There are no marked changes in the DIV across time for the two experimental conditions. (C-H) Extracted neuronal parameters averaged across recordings for the time periods during recordings (n = 6 for vehicle, n = 6 α-syn aggregates). Capacitance (C) showed no significant change over time for all the experimental conditions. (D) There was a small increase in whole-cell conductance for neurons with α-syn aggregates, but the percentage change was closer to vehicle than to α-syn aggregates without glibenclamide. Resting potential (F) and spike threshold (G) also slightly increased with time, the potential difference from rest potential to spike threshold remained constant with time. (H) Graph plotting the normalised conductance (normalised to the conductance at time 0 mins) for all experimental conditions. Using a Kruskal Wallis ANOVA, we confirmed that both time and experimental condition had a significant effect on conductance ($P < 0.0001$ and $P < 0.0001$ respectively). At 32 mins, the neurons with α-syn aggregates injected have a significantly greater conductance than any of the other experimental conditions (vs control $P < 0.0001$, vs monomer $P = 0.0003$, vs Glib + control $P < 0.0001$, vs Glib + aSyn $P = 0.0045$; Dunn's post hoc analysis). No other experimental conditions were significantly different from each other.

Table 1

	Vehicle/ control			aSyn aggregates			aSyn monomers			Glib + vehicle			Glib + aSyn aggregates		
Parameter	**Mean**	**SEM**	**SD**	**Mean**	**SEM**	**SD**	**Mean**	**SEM**	**SD**	**Mean**	**SEM**	**SD**	**Mean**	**SEM**	**SD**
RMP (mV)	-55.8	± 1.2	± 3.79	-55.4	± 1.23	± 4.10	-56.8	± 1.30	± 3.18	-53.2	± 2.14	± 5.24	-60.4	± 1.82	± 4.08
R in (MΩ)	338	± 17.6	± 55.8	312	± 17.1	± 56.8	359	± 42.2	± 103.3	386	± 25.2	± 61.7	294	± 41.9	± 93.6
Firing Rate (Hz)	1.63	± 0.39	± 0.12	2.51	± 1.57	± 0.47	2.38	± 1.14	± 0.46	2.27	± 1.15	± 0.47	2.04	± 1.29	± 0.52
C (pF)	88.8	± 5.74	± 14.1	107.8	± 5.84	± 14.3	80.73	± 15.1	± 37.0	81.16	± 8.54	± 20.9	117	± 22.3	± 54.7
g (nS)	2.29	± 0.2	± 0.49	2.78	± 0.2	± 0.49	1.99	± 0.3	± 0.73	2.39	± 0.29	± 0.71	3.67	± 0.55	± 1.35

Table 1: Electrophysiological parameters measured for dopaminergic neurons at time zero for all experimental treatments

Data	Figure	Statistical Test	Test values	P value
0 mins, all conditions, RMP	Figure 4	Kruskal-Wallis ANOVA	H (4) = 0.5385	P = 0.4657
0 mins, all conditions , IR	Figure 4	Kruskal-Wallis ANOVA	H (4) = 2.109	P = 0.2727
0 mins all conditions , FR	Figure 4	Kruskal-Wallis ANOVA	H (4) = 1.395	P = 0.8511
0 mins vs 32 mins, aSyn aggregates, IR	Figure 4	Wilcoxon signed-rank test	W(+) = 2.0, W(-) = 64.0, Z = 2.7	P = 0.0029
0 mins vs 32 mins, aSyn monomers, IR	Figure 4	Wilcoxon signed-rank test	W(+) = 6.5, W(-) = 14.5, Z = 0.73	P = 0.4688
0 mins vs 32 mins, vehicle, IR	Figure 4	Wilcoxon signed-rank test	W(+) = 46.0, W(-) = 9.0, Z = -1.83	P = 0.0645
32 mins, aSyn aggregates, aSyn monomers and vehicle, IR	Figure 4	Kruskal-Wallis ANOVA	H (2) = 14.53	P = 0.0007
16 mins, aSyn aggregates, aSyn monomers and vehicle, IR	Figure 4	Kruskal-Wallis ANOVA	H (2) = 10.67	P = 0.0048
0 mins vs 32 mins, vehicle, RMP	Figure 4	Wilcoxon signed-rank test	W(+) = 41.5, W(-) = 3.5, Z = -2.19	P = 0.0234
0 mins vs 32 mins, aSyn aggregates, RMP	Figure 4	Wilcoxon signed-rank test	W(+) = 61.0, W(-) = 5.0, Z = -2.44	P = 0.0107
0 mins vs 32 mins, aSyn monomers, RMP	Figure 4	Wilcoxon signed-rank test	W(+) = 19.5, W(-) = 1.5 Z = -1.79	P = 0.0938
32 mins, aSyn aggregates, aSyn monomers and vehicle, RMP	Figure 4	Kruskal-Wallis ANOVA	H (2) = 2.234	P = 0.3273
0 mins vs 32 mins, vehicle, FR	Figure 4	Wilcoxon signed-rank test	W(+) = 14, W(-) = 41.0 Z = -1.32	P = 0.1895
0 mins vs 32 mins, aSyn aggregates, FR	Figure 4	Wilcoxon signed-rank test	W(+) = 1.0, W(-) = 65.0 Z = 2.8	P = 0.0020
0 mins vs 32 mins, aSyn monomers, FR	Figure 4	Wilcoxon signed-rank test	W(+) = 11, W(-) = 10.0 Z = 0	P > 0.9999
32 mins, aSyn aggregates, aSyn monomers and vehicle, FR	Figure 4	Kruskal-Wallis ANOVA	H (2) = 10.21	P = 0.0061
0 mins, all conditions, capacitance	Figure 5	Kruskal-Wallis ANOVA	H (4) = 6.269	P = 0.18
0 mins vs 32 mins, aSyn aggregates, membrane conductance	Figure 5	Wilcoxon signed-rank test	W(+) = 66.0 , W(-) = 0 Z = -2.89	P = 0.001
0 mins vs 32 mins, vehicle, membrane conductance	Figure 5	Wilcoxon signed-rank test	W(+) = 71.0 , W(-) = 7 Z = -2.47	P = 0.009
32 mins, aSyn monomers and vehicle, membrane conductance	Figure 5	Mann-Whitney test	Vehicle median = 2.820, n=12, aSyn monomers = 2.820, n=6, U = 36	P > 0.9999
32 mins, aSyn aggregates and vehicle, membrane conductance	Figure 5	Mann-Whitney test	aSyn aggregates median = 6.450, n = 11,	P = 0.0003

eNeuro Accepted Manuscript

			vehicle median = 2.820, n = 12, U = 11	
0 mins, vehicle and vehicle + glib, RMP	Figure 6	Mann-Whitney test	Vehicle median = -56, n = 10, Vehicle + Glib median = -54, n = 6, U = 21.50	P = 0.3791
0 mins, vehicle and vehicle + glib, IR	Figure 6	Mann-Whitney test	Vehicle median = 338.3, n = 10, Vehicle + Glib median = 393, n = 6, U = 18.50	P = 0.2294
0 mins, vehicle and vehicle + glib, FR	Figure 6	Mann-Whitney test	Vehicle median = 69.5, n = 10, Vehicle + Glib median = 86.5, n = 6, U = 25.50	P = 0.6548
0 mins vs 32 mins, vehicle + glib, IR	Figure 6	Wilcoxon signed-rank test	W(+) = 9.0, W(-) = 12.0 Z = 0.21	P = 0.8438
0 mins vs 32 mins, vehicle + glib, FR	Figure 6	Wilcoxon signed-rank test	W(+) = 7.0, W(-) = 14.0 Z = 0.63	P = 0.5625
0 mins vs 32 mins, aSyn + glib, IR	Figure 6	Wilcoxon signed-rank test	W(+) = 5.0, W(-) = 16.0 Z = 1.04	P = 0.25
0 mins vs 32 mins, aSyn + glib, FR	Figure 6	Wilcoxon signed-rank test	W(+) = 7.0, W(-) = 14.0 Z = 0.63	P = 0.353
0 mins vs 32 mins, aSyn + glib, membrane conductance	Figure 7	Wilcoxon signed-rank test	W(+) = 21.0, W(-) = 0 Z = 0.63	P = 0.0313
32 mins, vehicle + glib and aSyn + glib, membrane conductance	Figure 7	Mann-Whitney test	Vehicle + glib median = 4.675, n = 6, aSyn + glib median = 3.33, n = 6, U = 11	P = 0.3095
Normalised conductance over time, all conditions Conductance effect Time effect aSyn aggregates vs control aSyn aggregates vs monomers aSyn aggregates vs vehicle + glib aSyn aggregates vs aSyn + Glib	Figure 7	Kruskal-Wallis ANOVA Dunn's Posthoc analysis	 F (4, 180) = 6.806 F (4, 180) = 11.01	 P < 0.0001 P < 0.0001 P < 0.0001 P = 0.0003 P < 0.0001 P = 0.0045

889

890 **Table 2:** A table of all of the statistical tests and associated results.

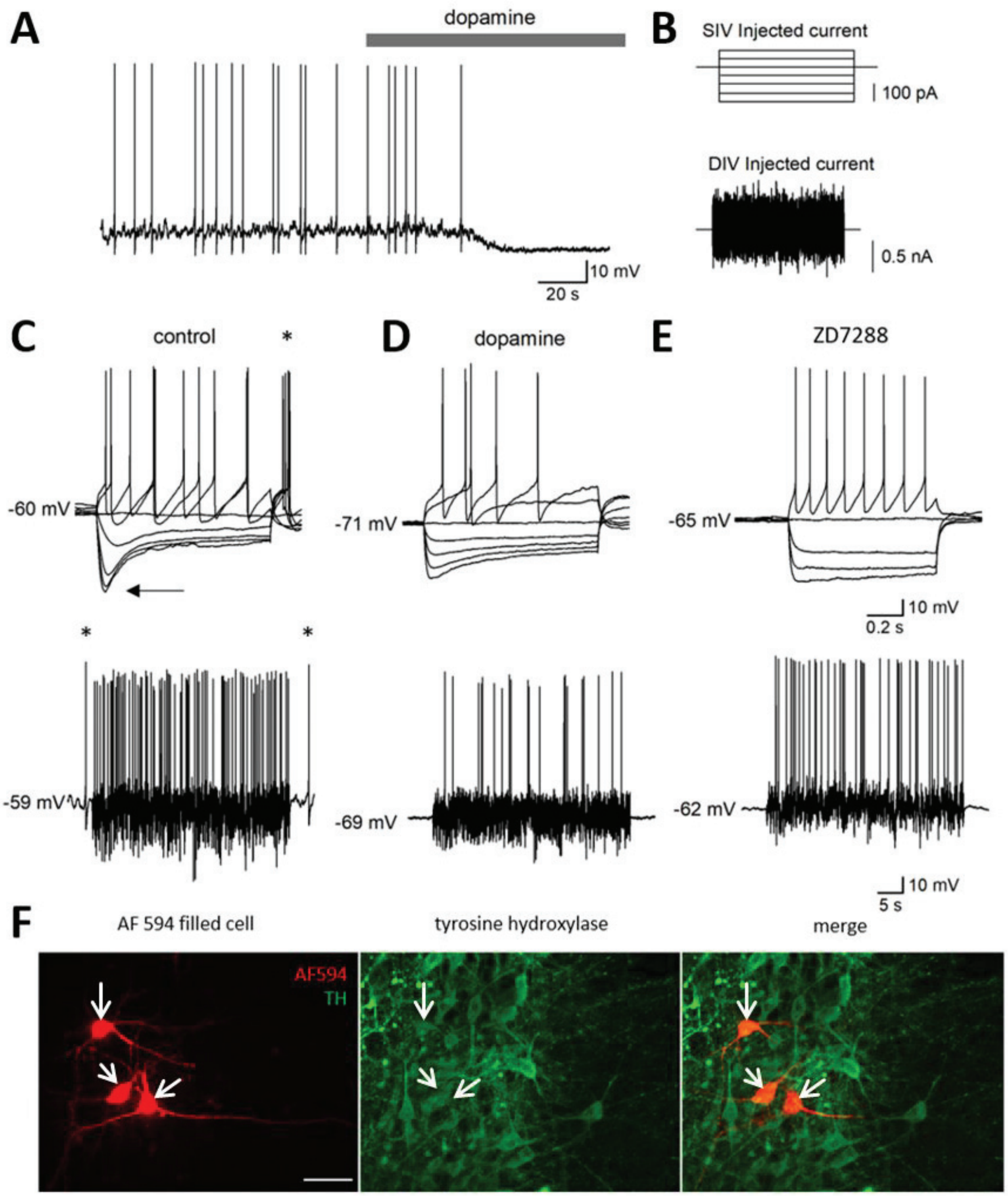
A
dopamine
10 mV
20 s
B
SIV Injected current
100 pA
DIV Injected current
0.5 nA
C
control
-60 mV
-59 mV
D
dopamine
-71 mV
-69 mV
E
ZD7288
-65 mV
10 mV
0.2 s
-62 mV
10 mV
5 s
F
AF 594 filled cell
tyrosine hydroxylase
merge
AF594
TH

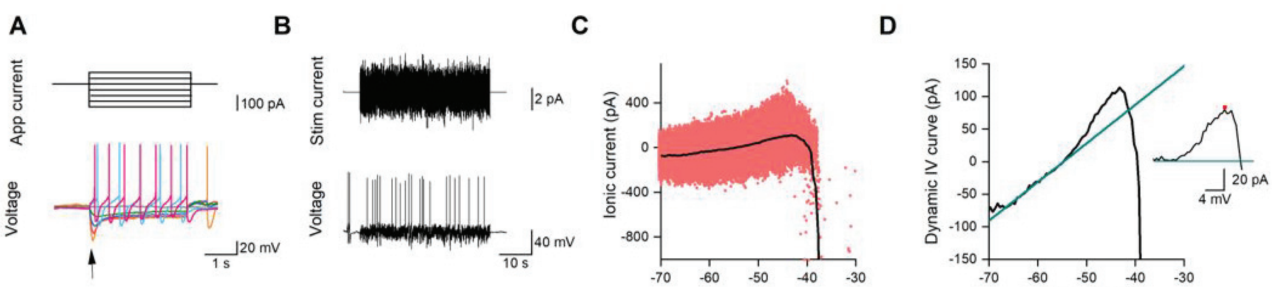
A
App current
100 pA
Voltage
20 mV
1 s
B
Stim current
2 pA
Voltage
40 mV
10 s
C
Ionic current (pA)
400
0
-400
-800
-70
-60
-50
-40
-30
Voltage (mV)
D
Dynamic IV curve (pA)
150
100
50
0
-50
-100
-150
-70
-60
-50
-40
-30
Voltage (mV)
20 pA
4 mV

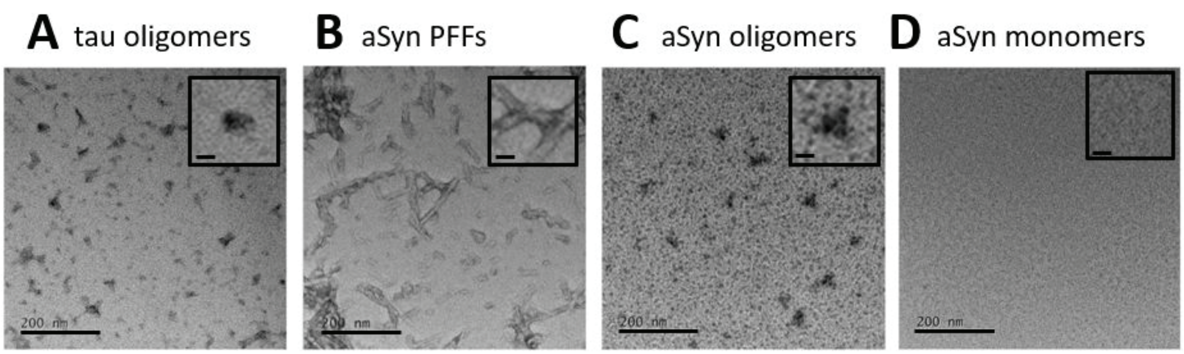
A tau oligomers
B aSyn PFFs
C aSyn oligomers
D aSyn monomers
200 nm
200 nm
200 nm
200 nm

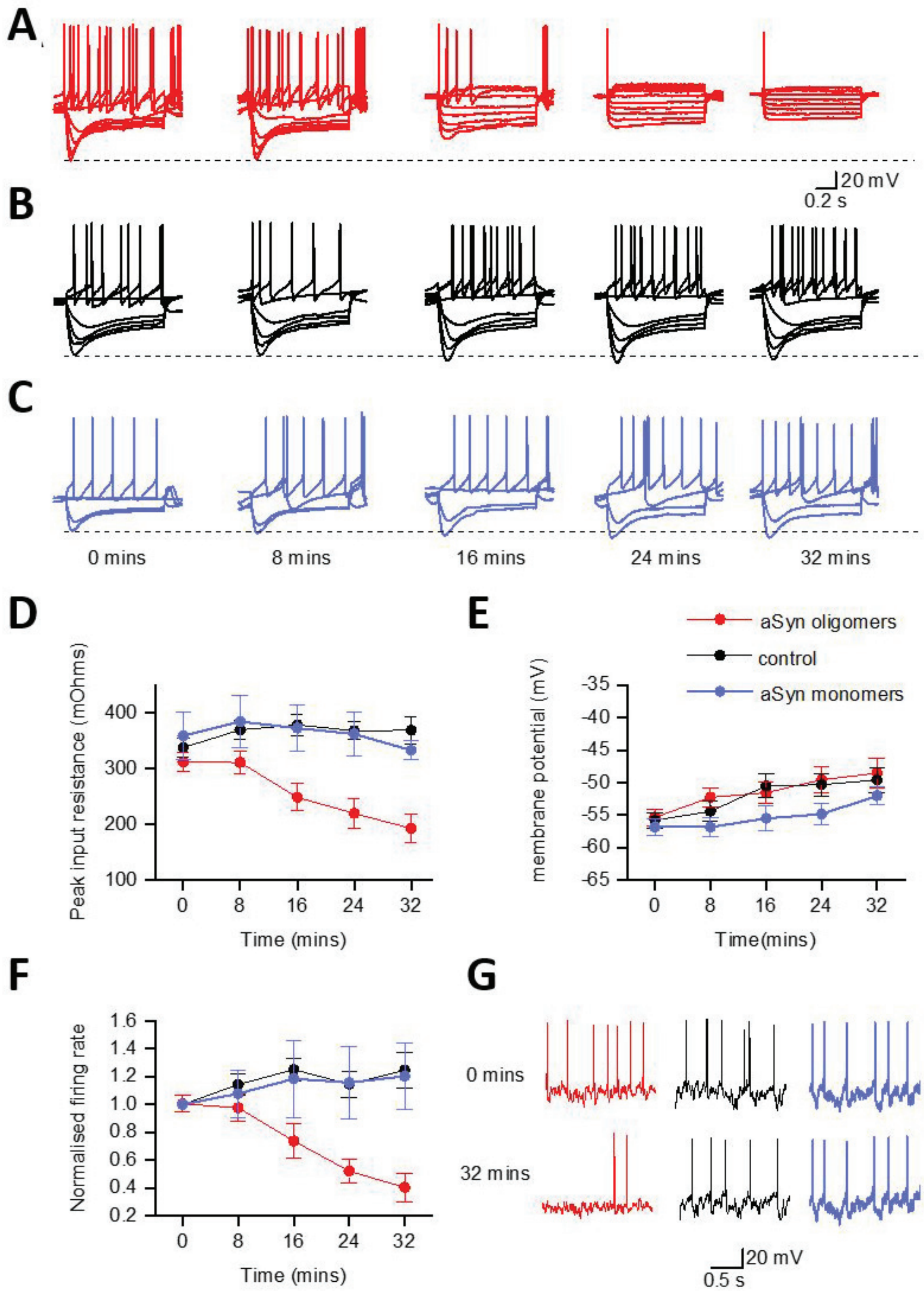
A
20 mV
0.2 s
B
C
0 mins
8 mins
16 mins
24 mins
32 mins
D
Peak input resistance (mOhms)
Time (mins)
E
aSyn oligomers
control
aSyn monomers
membrane potential (mV)
Time(mins)
F
Normalised firing rate
Time (mins)
G
0 mins
32 mins
20 mV
0.5 s

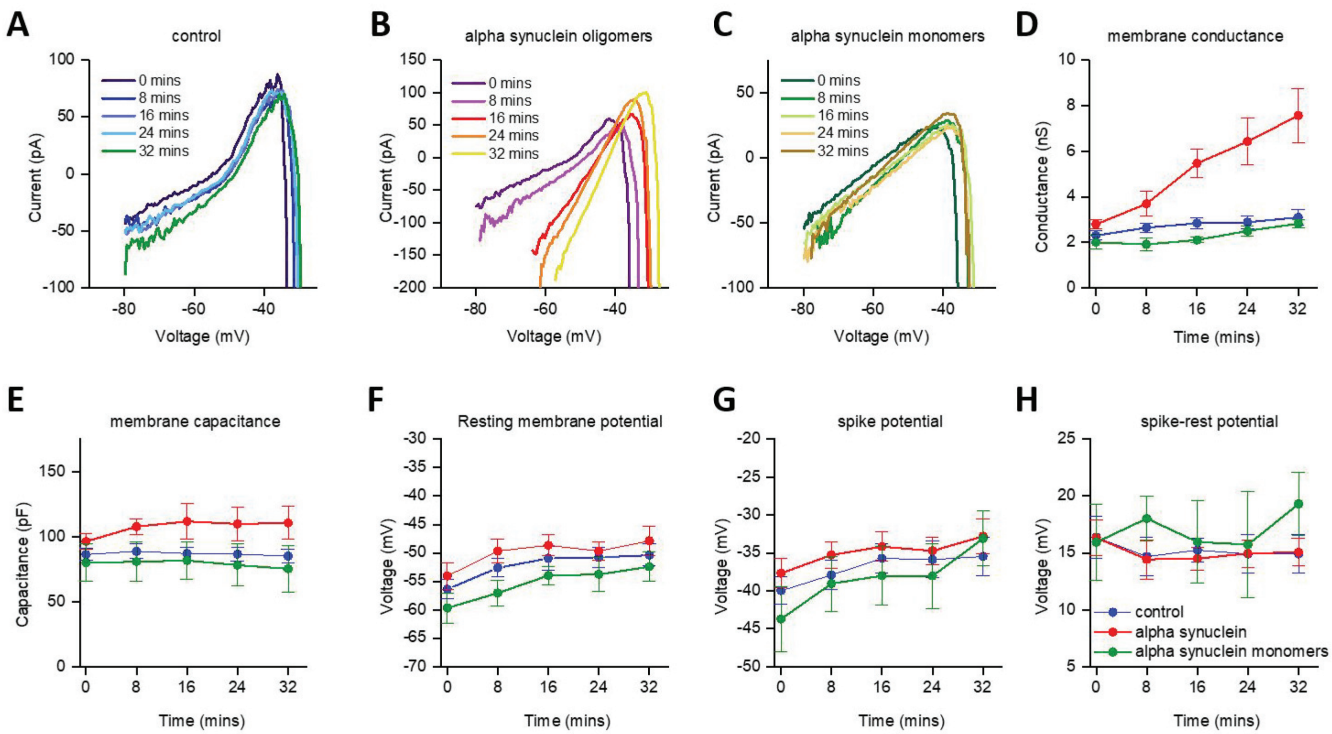
A
control
Current (pA)
Voltage (mV)
0 mins
8 mins
16 mins
24 mins
32 mins
B
alpha synuclein oligomers
Current (pA)
Voltage (mV)
0 mins
8 mins
16 mins
24 mins
32 mins
C
alpha synuclein monomers
Current (pA)
Voltage (mV)
0 mins
8 mins
16 mins
24 mins
32 mins
D
membrane conductance
Conductance (nS)
Time (mins)
E
membrane capacitance
Capacitance (pF)
Time (mins)
F
Resting membrane potential
Voltage (mV)
Time (mins)
G
spike potential
Voltage (mV)
Time (mins)
H
spike-rest potential
Voltage (mV)
Time (mins)
control
alpha synuclein
alpha synuclein monomers

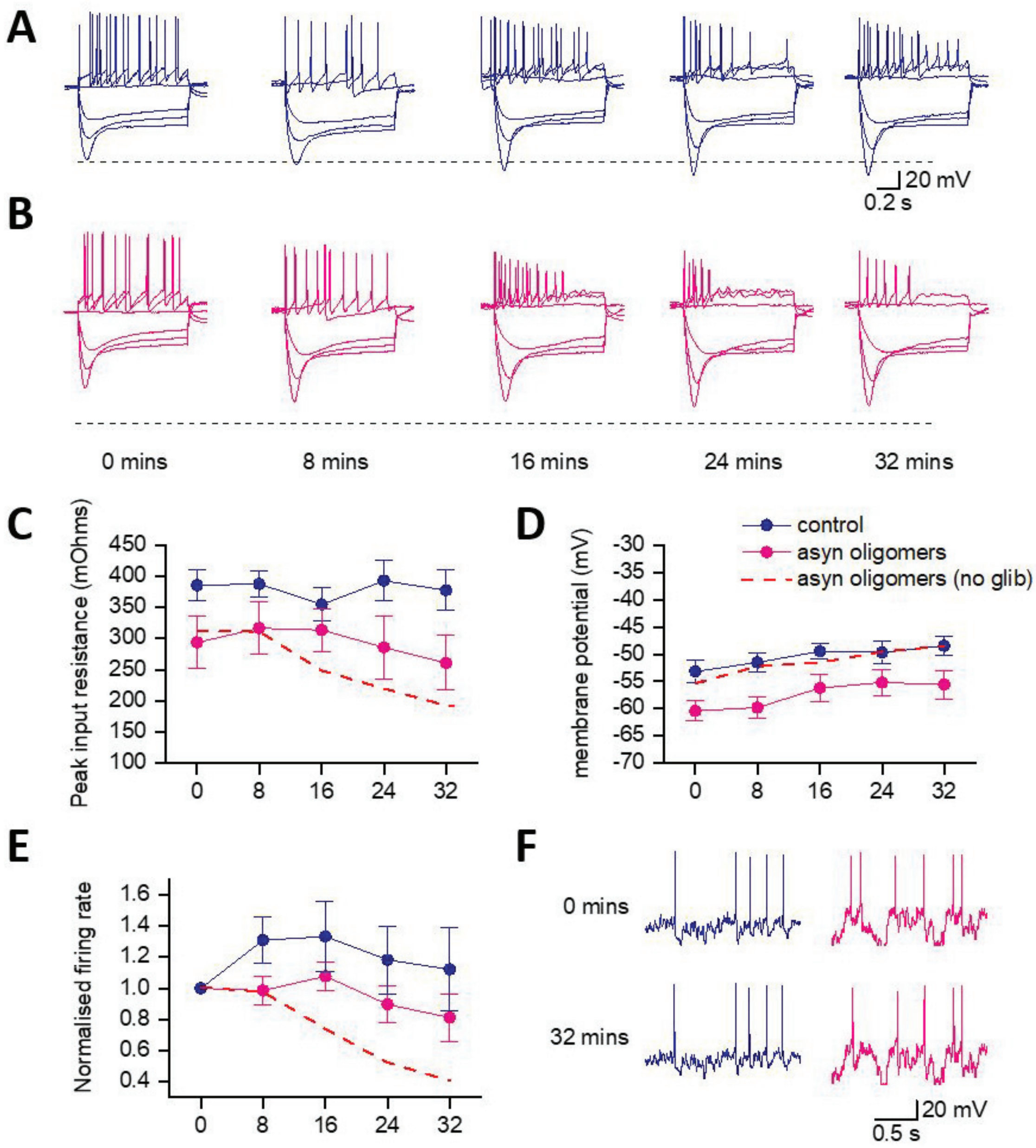
A
B
20 mV
0.2 s
0 mins
8 mins
16 mins
24 mins
32 mins
C
Peak input resistance (mOhms)
D
membrane potential (mV)
control
asyn oligomers
asyn oligomers (no glib)
E
Normalised firing rate
F
0 mins
32 mins
20 mV
0.5 s

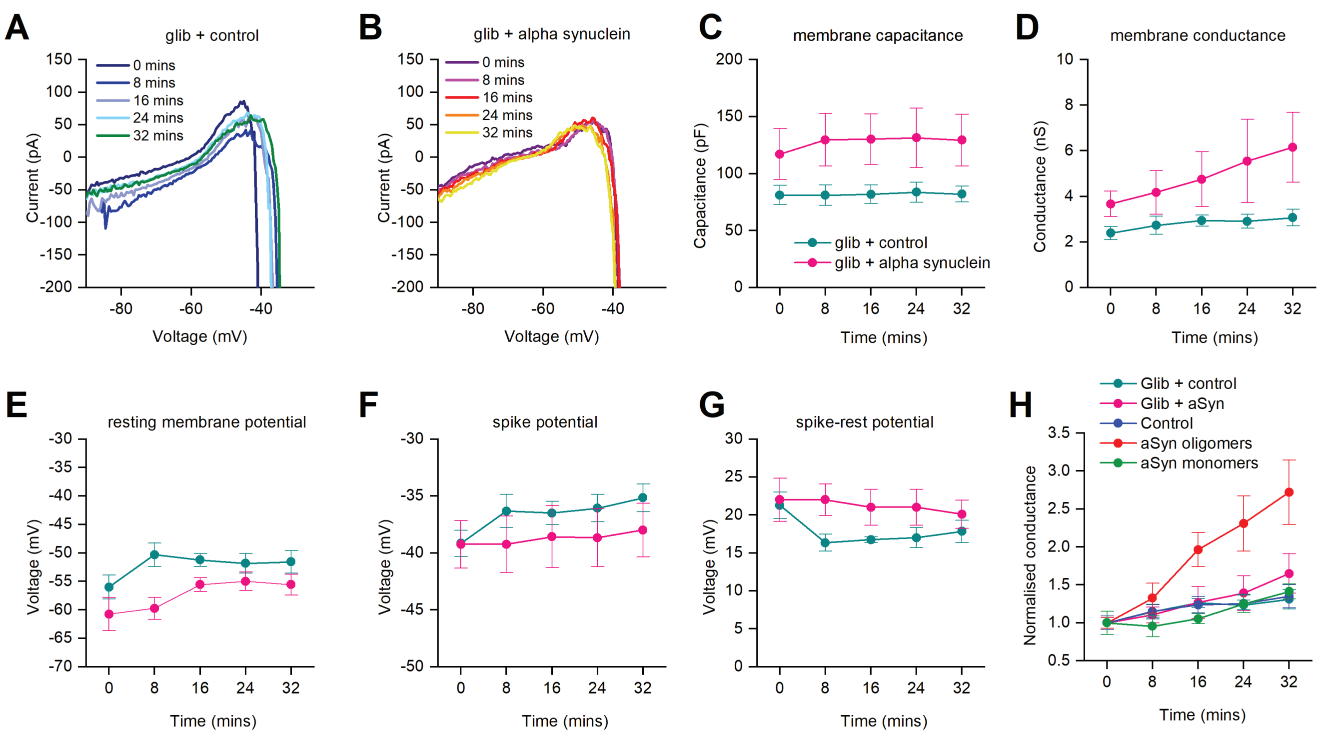
A
glib + control
0 mins
8 mins
16 mins
24 mins
32 mins
Current (pA)
Voltage (mV)
B
glib + alpha synuclein
C
membrane capacitance
Capacitance (pF)
glib + control
glib + alpha synuclein
Time (mins)
D
membrane conductance
Conductance (nS)
E
resting membrane potential
Voltage (mV)
F
spike potential
G
spike-rest potential
H
Glib + control
Glib + aSyn
Control
aSyn oligomers
aSyn monomers
Normalised conductance

Table 1

	Vehicle/ control			aSyn aggregates			aSyn monomers			Glib + vehicle			Glib + aSyn aggregates		
Parameter	**Mean**	**SEM**	**SD**	**Mean**	**SEM**	**SD**	**Mean**	**SEM**	**SD**	**Mean**	**SEM**	**SD**	**Mean**	**SEM**	**SD**
RMP (mV)	-55.8	± 1.2	± 3.79	-55.4	± 1.23	± 4.10	-56.8	± 1.30	± 3.18	-53.2	± 2.14	± 5.24	-60.4	± 1.82	± 4.08
R in (MΩ)	338	± 17.6	± 55.8	312	± 17.1	± 56.8	359	± 42.2	± 103.3	386	± 25.2	± 61.7	294	± 41.9	± 93.6
Firing Rate (Hz)	1.63	± 0.39	± 0.12	2.51	± 1.57	± 0.47	2.38	± 1.14	± 0.46	2.27	± 1.15	± 0.47	2.04	± 1.29	± 0.52
C (pF)	88.8	± 5.74	± 14.1	107.8	± 5.84	± 14.3	80.73	± 15.1	± 37.0	81.16	± 8.54	± 20.9	117	± 22.3	± 54.7
g (nS)	2.29	± 0.2	± 0.49	2.78	± 0.2	± 0.49	1.99	± 0.3	± 0.73	2.39	± 0.29	± 0.71	3.67	± 0.55	± 1.35

Table 1: Electrophysiological parameters measured for dopaminergic neurons at time zero for all experimental treatments